Research Article | Vol. 8, No. 6 | 1 Jun 2018 | OPTICAL MATERIALS EXPRESS 1650
Optical Materials EXPRESS

Nd^{3+}:Ga-Ge-Sb-S glasses and fibers for luminescence in mid-IR: synthesis, structural characterization and rare earth spectroscopy

R. CHAHAL,[1] F. STARECKI,[1,2] J.-L. DOUALAN,[2] P. NĚMEC,[3] A. TRAPANANTI,[4] C. PRESTIPINO,[1] G. TRICOT,[5] C. BOUSSARD-PLEDEL,[1] K. MICHEL,[6] A. BRAUD,[2] P. CAMY,[2] J.-L. ADAM,[1] B. BUREAU,[1] AND V. NAZABAL[1,*]

[1]*ISCR, UMR-CNRS 6226 Université de Rennes 1, 35042 Rennes, France*
[2]*CIMAP, UMR 6252 CEA-CNRS-ENSI Caen, Université de Caen, 14050 Caen, France*
[3]*Faculty of Chemical Technology, University of Pardubice, 53210 Pardubice, Czech Republic*
[4]*CNR-IOM-OGG c/o ESRF, F-38043 Grenoble, France*
[5]*UCCS, UMR 8181, ENSCL-C7, Université de Lille 1 – 59655 Villeneuve d'Ascq, France*
[6]*Bureau de Recherches Géologiques & Minières, F – 45060 Orléans, France*
**virginie.nazabal@univ-rennes1.fr*

Abstract: With high refractive indices, appropriate solubility of rare earth, low phonon energy and transparency from the visible to 10 µm, a Ga-Ge-Sb-S system allows emission from Nd^{3+} ions in the near- and mid-IR spectral ranges. The glass transition temperature, density, expansion coefficient, and near and mid-IR refractive indexes were measured on bulk samples. Their glass network structures were analyzed by Raman scattering spectrometry, NMR of ^{71}Ga and extended X-ray absorption fine structure (EXAFS, K-edge of Ga, Ge, Sb, S and Nd). The absorption and emission spectra of neodymium doped sulfide glasses were recorded from the visible to the mid-IR. Excited state lifetimes were measured for several transitions. The lifetimes decrease with the concentration of Nd^{3+}, especially for the $^4I_{13/2}$ and $^4I_{11/2}$ levels. The spectroscopic parameters were determined by the Judd-Ofelt method, allowing the calculation of cross-section emissions and the evaluation of quantum yields. Optical attenuation and emission measurements of fiber were also performed with a broad 4.7-5.7 µm emission band in the mid-IR.

OCIS codes: (160.2290) Fiber materials; (160.2540) Fluorescent and luminescent materials; (160.2750) Glass and other amorphous materials; (160.5690) Rare-earth-doped materials; (300.1030) Absorption; (300.2140) Emission; (300.6280) Spectroscopy, fluorescence and luminescence.

References and links

1. J. S. Sanghera and I. D. Aggarwal, "Active and passive chalcogenide glass optical fibers for IR applications: a review," J. Non-Cryst. Solids **257**, 6–16 (1999).
2. M. F. Churbanov, I. V. Scripachev, V. S. Shiryaev, V. G. Plotnichenko, S. V. Smetanin, E. B. Pyrkov, and Y. N. Galagan, "Chalcogenide glasses doped with Tb, Dy and Pr ions," J. Non-Cryst. Solids **326**, 301–305 (2003).
3. J. Heo, "Rare-earth doped chalcogenide glasses for fiber-optic amplifiers," J. Non-Cryst. Solids **326-327**, 410–415 (2003).
4. T. Schweizer, D. W. Hewak, B. N. Samson, and D. N. Payne, "Spectroscopy of potential mid-infrared laser transitions in gallium lanthanum sulphide glass," J. Lumin. **72–74**, 419–421 (1997).
5. J. S. Sanghera, L. B. Shaw, L. E. Busse, V. Q. Nguyen, P. C. Pureza, B. C. Cole, B. B. Harbison, I. D. Aggarwal, R. Mossadegh, F. Kung, D. Talley, D. Roselle, and R. Miklos, "Development and infrared applications of chalcogenide glass optical fibers," Fiber Integr. Opt. **19**(3), 251–274 (2000).
6. D. J. Lee, J. Heo,and S. H. Park, "Energy transfer and 1.48 mu m emission properties in chalcohalide glasses doped with Tm^{3+} and Tb^{3+}," J. Non-Cryst. Solids **331**, 184–189 (2003).
7. M. Ichikawa, Y. Ishikawa, T. Wakasugi, and K. Kadono, "Near- and mid-infrared emissions from Dy^{3+} and Nd^{3+}-doped Ga_2S_3-GeS_2-Sb_2S_3 glass," Opt. Mater. **35**(11), 1914–1917 (2013).
8. H. Sakr, Z. Tang, D. Furniss, L. Sojka, S. Sujecki, T. M. Benson, and A. B. Seddon, "Promising emission behavior in Pr^{3+}/In selenide-chalcogenide-glass small-core step index fiber (SIF)," Opt. Mater. **67**, 98–107 (2017).

#326232 https://doi.org/10.1364/OME.8.001650
Journal © 2018 Received 19 Mar 2018; revised 6 May 2018; accepted 7 May 2018; published 30 May 2018

Optical Materials EXPRESS

9. B. J. Park, H. S. Seo, J. T. Ahn, Y. G. Choi, J. Heo, and W. J. Chung, "Dy^{3+} doped Ge-Ga-Sb-Se glasses and optical fibers for the mid-IR gain media," J. Ceram. Soc. Jpn. **116**(1358), 1087–1091 (2008).
10. B. J. Park, H. S. Seo, J. T. Ahn, Y. G. Choi, D. Y. Jeon, and W. J. Chung, "Mid-infrared (3.5-5.5 μm) spectroscopic properties of Pr^{3+}-doped Ge-Ga-Sb-Se glasses and optical fibers," J. Lumin. **128**(10), 1617–1622 (2008).
11. F. Starecki, N. Abdellaoui, A. Braud, J.-L. Doualan, C. Boussard-Plédel, B. Bureau, P. Camy, and V. Nazabal, "8 μm luminescence from a Tb^{3+} GaGeSbSe fiber," Opt. Lett. **43**(6), 1211–1214 (2018).
12. R. Chahal, F. Starecki, C. Boussard-Plédel, J.-L. Doualan, K. Michel, L. Brilland, A. Braud, P. Camy, B. Bureau, and V. Nazabal, "Fiber evanescent wave spectroscopy based on IR fluorescent chalcogenide fibers," Sens. Actuators B Chem. **229**, 209–216 (2016).
13. F. Starecki, S. Morais, R. Chahal, C. Boussard-Plédel, B. Bureau, F. Palencia, C. Lecoutre, Y. Garrabos, S. Marre, and V. Nazabal, "IR emitting Dy^{3+} doped chalcogenide fibers for in situ CO_2 monitoring in high pressure microsystems," Int. J. Greenh. Gas Control **55**, 36–41 (2016).
14. F. Starecki, F. Charpentier, J. L. Doualan, L. Quetel, K. Michel, R. Chahal, J. Troles, B. Bureau, A. Braud, P. Camy, V. Moizan, and V. Nazabal, "Mid-IR optical sensor for CO_2 detection based on fluorescence absorbance of Dy^{3+}:$Ga_5Ge_{20}Sb_{10}S_{65}$ fibers," Sens. Actuators B Chem. **207**, 518–525 (2015).
15. M. Ichikawa, Y. Ishikawa, T. Wakasugi, and K. Kadono, "Mid-infrared emissions from Er^{3+} in $Ga_{(2)}S_{(3)}$-GeS_2-Sb_2S_3 glasses," J. Mater. Res. **25**(11), 2111–2119 (2010).
16. A. Belykh, L. Glebov, C. Lerminiaux, S. Lunter, M. Mikhailov, A. Plyukhin, M. Prassas, and A. Przhevuskii, "Spectral and luminescence properties of neodymium in chalcogenide glasses," J. Non-Cryst. Solids **213-214**, 238–244 (1997).
17. H. Takebe, T. Ishibashi, T. Ichiki, and K. Morinaga, "Nd solubility in RS-Ga_2S_3 (R = Sr, Ba) glasses," J. Ceram. Soc. Jpn. **111**(1298), 755–757 (2003).
18. B. G. Aitken, C. W. Ponader, and R. S. Quimby, "Clustering of rare earths in GeAs sulfide glass," C. R. Chim. **5**(12), 865–872 (2002).
19. L. Bodiou, F. Starecki, J. Lemaitre, V. Nazabal, J.-L. Doualan, E. Baudet, R. Chahal, A. Gutierrez-Arroyo, Y. Dumeige, I. Hardy, A. Braud, R. Soulard, P. Camy, P. Nemec, G. Palma, F. Prudenzano, and J. Charrier, "Mid-infrared guided photoluminescence from integrated Pr_{3+}-doped selenide ridge waveguides," Opt. Mater. **75**, 109–115 (2018).
20. G. Le Caer, B. Bureau, and D. Massiot, "An extension of the Czjzek model for the distributions of electric field gradients in disordered solids and an application to NMR spectra of Ga-71 in chalcogenide glasses," J. Phys.-.Condes. Matter **22**, 17 (2010).
21. Y. Ledemi, B. Bureau, G. Le Caer, L. Calvez, C. Roiland, G. Tricot, P. Florian, V. Nazabal, and D. Massiot, "Ga-71 NMR in chalcogenide and chalco-halide glasses," J. Non-Cryst. Solids **383**, 216–221 (2014).
22. B. R. Judd, "Optical absorption intensities of rare earth ions," Phys. Rev. **127**(3), 750–761 (1962).
23. G. S. Ofelt, "Intensities of crystal spectra of rare earth ions," J. Chem. Phys. **37**(3), 511–520 (1962).
24. J. Kobelke, J. Kirchhof, K. Schuster, and A. Schwuchow, "Effects of carbon, hydrocarbon and hydroxide impurities on praseodymium doped arsenic sulfide based glasses," J. Non-Cryst. Solids **284**(1-3), 123–127 (2001).
25. M. F. Churbanov, I. V. Scripachev, G. E. Snopatin, V. S. Shiryaev, and V. G. Plotnichenko, "High-purity glasses based on arsenic chalcogenides," J. Optoelectron. Adv. Mater. **3**, 341–349 (2001).
26. P. Nemec, M. Olivier, E. Baudet, A. Kalendova, P. Benda, and V. Nazabal, "Optical properties of $(GeSe_2)_{(100-x)}(Sb_2Se_3)_{(x)}$ glasses in near- and middle-infrared spectral regions," Mater. Res. Bull. **51**, 176–179 (2014).
27. K. Jinguji, M. Horiguchi, and T. Manabe, "Spectral loss measurement system for IR optical fibers," Appl. Opt. **21**(4), 571–572 (1982).
28. R. W. G. R. Shuker and R. W. Gammon, "Raman-scattering selection-rule breaking and the density of states in amophous materials," Phys. Rev. Lett. **25**(4), 222–225 (1970).
29. C. Julien, S. Barnier, M. Massot, N. Chbani, X. Cai, A. M. Loireaulozach, and M. Guittard, "Raman and Infrared Spectroscopic Studies of Ge-Ga-Ag Sulfide Glasses," Materials Science and Engineering B-Solid State Materials for Advanced Technology **22**(2-3), 191–200 (1994).
30. K. V. Klementev, "Extraction of the fine structure from X-ray absorption spectra," J. Phys. D Appl. Phys. **34**(2), 209–217 (2001).
31. A. L. Ankudinov, B. Ravel, J. J. Rehr, and S. D. Conradson, "Real-space multiple-scattering calculation and interpretation of X-ray-absorption near-edge structure," Phys. Rev. B **58**(12), 7565–7576 (1998).
32. Y. Nakane, H. Nasu, J. Heo, T. Hashimoto, and K. Kamiya, "Second harmonic generation from thermally poled Ge-S glass system," J. Ceram. Soc. Jpn. **113**(1323), 728–732 (2005).
33. J. Chovanec, M. Chromcikova, M. Liska, J. Shanelova, and J. Malek, "Thermodynamic model and viscosity of Ge-S glasses," J. Therm. Anal. Calorim. **116**(2), 581–588 (2014).
34. J. Malek, J. Chovanec, R. Svoboda, Y. Taniguchi, and H. Kawaji, "Heat capacity of vitreous GeS_2," J. Chem. Thermodyn. **81**, 101–108 (2015).
35. J. Troles, Y. Niu, C. Duverger-Arfuso, F. Smektala, L. Brilland, V. Nazabal, V. Moizan, F. Desevedavy, and P. Houizot, "Synthesis and characterization of chalcogenide glasses from the system Ga-Ge-Sb-S and preparation of a single-mode fiber at 1.55 μm," Mater. Res. Bull. **43**(4), 976–982 (2008).
36. J. L. Z. Adam, *Chalcogenide Glasses, Preparation, Properties and Applications* (Woodhead Publishing Limited, 2014).

Optical Materials EXPRESS

37. A. B. Seddon, "Chalcogenide Glasses - a Review of Their Preparation, Properties and Applications," J. Non-Cryst. Solids **184**, 44–50 (1995).
38. Y. Yang, Z. Yang, P. Lucas, Y. Wang, Z. Yang, A. Yang, B. Zhang, and H. Tao, "Composition dependence of physical and optical properties in Ge-As-S chalcogenide glasses," J. Non-Cryst. Solids **440**, 38–42 (2016).
39. A. Bytchkov, G. J. Cuello, S. Kohara, C. J. Benmore, D. L. Price, and E. Bychkov, "Unraveling the atomic structure of Ge-rich sulfide glasses," Phys. Chem. Chem. Phys. **15**(22), 8487–8494 (2013).
40. H. Takebe, T. Hirakawa, T. Ichiki, and K. Morinaga, "Thermal stability and structure of Ge-Sb-S glasses," J. Ceram. Soc. Jpn. **111**(1296), 572–575 (2003).
41. L. Petit, N. Carlie, F. Adamietz, M. Couzi, V. Rodriguez, and K. C. Richardson, "Correlation between physical, optical and structural properties of sulfide glasses in the system Ge-Sb-S," Mater. Chem. Phys. **97**(1), 64–70 (2006).
42. A. M. Loireau-Lozach, F. Keller-Besrest, and S. Bénazeth, "Short and medium range order in Ga-Ge-S glasses: An X-ray absorption spectroscopy study at room and low temperatures," J. Solid State Chem. **123**(1), 60–67 (1996).
43. P. Masselin, D. Le Coq, A. Cuisset, and E. Bychkov, "Spatially resolved Raman analysis of laser induced refractive index variation in chalcogenide glass," Opt. Mater. Express **2**(12), 1768–1775 (2012).
44. A. Povolotskiy, T. Ivanova, A. Manshina, Y. Tver'yanovich, S. K. Liaw, and C. L. Chang, "Er^{3+} as glass structure modifier of Ga-Ge-S chalcogenide system," Appl. Phys., A Mater. Sci. Process. **96**(4), 887–891 (2009).
45. J. H. Song, Y. G. Choi, and J. Heo, "Ge and GaK-edge EXAFS analyses on the structure of Ge-Ga-S-CsBr glasses," J. Non-Cryst. Solids **352**(5), 423–428 (2006).
46. M. R. Davolos, A. Garcia, C. Fouassier, and P. Hagenmuller, "Luminescence of Eu^{2+} in strontium and barium thiogallates," J. Solid State Chem. **83**(2), 316–323 (1989).
47. A. Garcia, F. Guillen, and C. Fouassier, "Charge-transfer excitation of the Nd^{3+}, Sm^{3+}, Dy^{3+}, Ho^{3+}, Er^{3+}, and Tm^{3+} emission $CaGa_2S_4$," J. Lumin. **33**(1), 15–27 (1985).
48. R. E. Youngman and B. G. Aitken, "Structure and properties of GeGaP sulfide glasses," J. Non-Cryst. Solids **345-346**, 50–55 (2004).
49. A. W. Mao, B. G. Aitken, R. E. Youngman, D. C. Kaseman, and S. Sen, "Structure of Glasses in the Pseudobinary System Ga_2Se_3-$GeSe_2$: Violation of Chemical Order and 8-N Coordination Rule," J. Phys. Chem. B **117**(51), 16594–16601 (2013).
50. G. Lucovsky, J. P. deNeufville, and F. L. Galeener, "Study of optic modes of Ge0.30S0.70 glass by infrared and Raman spectroscopy," Phys. Rev. B **9**(4), 1591–1597 (1974).
51. S. Sugai, "Stochastic random network model in Ge and Si chalcogenide glasses," Phys. Rev. B Condens. Matter **35**(3), 1345–1361 (1987).
52. S. D. Pangavhane, P. Němec, V. Nazabal, A. Moreac, P. Jóvári, and J. Havel, "Laser desorption ionization time-of-flight mass spectrometry of erbium-doped Ga-Ge-Sb-S glasses," Rapid Commun. Mass Spectrom. **28**(11), 1221–1232 (2014).
53. B. Liu, Z. T. Song, T. Zhang, S. L. Feng, and B. M. Chen, "Raman spectra and XPS studies of phase changes in $Ge_2Sb_2Te_5$ films," Chin. Phys. **13**(11), 1947–1950 (2004).
54. W. H. Wei, L. Fang, X. Shen, and R. P. Wang, "Transition threshold in $Ge_xSb_{10}Se_{90-x}$ glasses," J. Appl. Phys. **115**(11), 113510 (2014).
55. M. Guignard, V. Nazabal, F. Smektala, J. L. Adam, O. Bohnke, C. Duverger, A. Moreac, H. Zeghlache, A. Kudlinski, G. Martinelli, and Y. Quiquempois, "Chalcogenide glasses based on germanium disulfide for second harmonic generation," Adv. Funct. Mater. **17**(16), 3284–3294 (2007).
56. T. S. Kavetskyy, "Radiation-induced structural changes in chalcogenide glasses as revealed from Raman spectroscopy measurements," Semiconductor Physics, Quantum Electronics & Optoelectronics **16**(1), 27–36 (2013).
57. V. Nazabal, P. Nemec, A. M. Jurdyc, S. Zhang, F. Charpentier, H. Lhermite, J. Charrier, J. P. Guin, A. Moreac, M. Frumar, and J. L. Adam, "Optical waveguide based on amorphous Er^{3+}-doped Ga-Ge-Sb-S(Se) pulsed laser deposited thin films," Thin Solid Films **518**(17), 4941–4947 (2010).
58. H. Higuchi, R. Kanno, Y. Kawamoto, M. Takahashi, and K. Kadono, "Local structures of Er^{3+} containing Ga_2S_3-GeS_2-La_2S_3 glass," Phys. Chem. Glasses **40**, 122–125 (1999).
59. I. D. Brown, "The bond-valence method: an empirical approach to chemical structure and bonding," Structure and Bonding in Crystals **II**, 1–30 (1981).
60. M. Fabian, E. Svab, V. Pamukchieva, A. Szekeres, K. Todorova, S. Vogel, and U. Ruett, "Reverse Monte Carlo modeling of the neutron and X-ray diffraction data for new chalcogenide Ge-Sb-S(Se)-Te glasses," J. Phys. Chem. Solids **74**(10), 1355–1362 (2013).
61. F. Charpentier, F. Starecki, J. L. Doualan, P. Jóvári, P. Camy, J. Troles, S. Belin, B. Bureau, and V. Nazabal, "Mid-IR luminescence of Dy^{3+} and Pr^{3+} doped $Ga_5Ge_{20}Sb_{10}S(Se)_{65}$ bulk glasses and fibers," Mater. Lett. **101**, 21–24 (2013).
62. Q. H. Yang, S. Z. Lu, B. Zhang, H. J. Zhang, J. Zhou, Z. J. Yuan, Y. F. Qi, and Q. H. Lou, "Preparation and laser performance of Nd-doped yttrium lanthanum oxide transparent ceramic," Opt. Mater. **33**(5), 692–694 (2011).
63. A. K. Mairaj, A. M. Chardon, D. P. Shepherd, and D. W. Hewak, "Laser performance and spectroscopic analysis of optically written channel waveguides in neodymium-doped gallium lanthanum sulphide glass," IEEE J. Sel. Top. Quantum Electron. **8**(6), 1381–1388 (2002).

Optical Materials EXPRESS

64. W. T. Carnall, P. R. Fields, and K. Rajnak, "Electronic energy levels in trivalent lanthanide aquo ions. I Pr^{3+} Nd^{3+} Pm^{3+} Sm^{3+} Dy^{3+} Ho^{3+} Er^{3+} and Tm^{3+}," J. Chem. Phys. **49**(10), 4424–4442 (1968).
65. K. Kadono, M. Shojiya, M. Takahashi, H. Higuchi, and Y. Kawamoto, "Radiative and non-radiative relaxation of rare-earth ions in Ga_2S_3–GeS_2–La_2S_3 glasses," J. Non-Cryst. Solids **259**(1-3), 39–44 (1999).
66. S. Tanabe, "Optical transitions of rare earth ions for amplifiers: how the local structure works in glass," J. Non-Cryst. Solids **259**(1-3), 1–9 (1999).
67. A. L. Pelé, A. Braud, J. L. Doualan, R. Chahal, V. Nazabal, C. Boussard-Plédel, B. Bureau, R. Moncorgé, and P. Camy, "Wavelength conversion in Er^{3+} doped chalcogenide fibers for optical gas sensors," Opt. Express **23**(4), 4163–4172 (2015).
68. J. L. Adam, J. L. Doualan, L. Griscom, S. Girard, and R. Moncorge, "Excited-state absorption at 1.3 μm in Nd^{3+}-doped fluoride and sulfide glasses," J. Non-Cryst. Solids **256-257**, 276–281 (1999).
69. A. D. Sontakke and K. Annapurna, "Spectroscopic properties and concentration effects on luminescence behavior of Nd^{3+} doped Zinc-Boro-Bismuthate glasses," Mater. Chem. Phys. **137**(3), 916–921 (2013).
70. A. D. Sontakke, K. Biswas, A. K. Mandal, and K. Annapurna, "Concentration quenched luminescence and energy transfer analysis of Nd^{3+} ion doped Ba-Al-metaphosphate laser glasses," Appl. Phys. B-Lasers Opt. **101**(1-2), 235–244 (2010).
71. V. Moizan, V. Nazabal, J. Troles, P. Houizot, J. L. Adam, J. L. Doualan, R. Moncorge, F. Smektala, G. Gadret, S. Pitois, and G. Canat, "Er^{3+}-doped GeGaSbS glasses for mid-IR fibre laser application: Synthesis and rare earth spectroscopy," Opt. Mater. **31**(1), 39–46 (2008).

1. Introduction

Chalcogenide glasses are interesting materials due to their wide glass formation region, optical transparency window and high refractive indices. They are also well known as host materials for rare earth ions [1–4]. They possess low phonon energy (~300-450 cm^{-1} for sulfides, ~200-350 cm^{-1} for selenides and 150-250 cm^{-1} for tellurides) that limits the non-radiative multiphonon relaxation rates. All these properties result in high quantum efficiencies for rare earth ion transitions in chalcogenide and chalcohalide glasses.

Many radiative transitions in the near-IR or middle-IR (mid-IR) have been observed in bulk chalcogenide glasses doped, for instance, with Pr^{3+}, Tb^{3+}, Dy^{3+}, Ho^{3+}, Er^{3+}, Nd^{3+} and Tm^{3+} ions [5–15]. Usually, Ge-Ga-As(Sb)-S sulfide systems are selected for enabling efficient fluorescence of rare earth ions. The quaternary Ga-Ge-Sb-S glass system doped with Nd^{3+} ions was selected to avoid the presence of arsenic. This system contains gallium, which allows a better solubility of RE^{3+} ions than other chalcogenide matrices without gallium [16–19]. Among this quaternary system, the nominal composition of $Ga_5Ge_{20}Sb_{10}S_{65}$ was especially preferred for its stability against crystallization and suitable thermo-mechanical properties favoring fiber drawing. The major interest of neodymium resides in its relatively distant and very wide emission in the mid-IR expected to occur between 4.7 and 5.7 μm relevant for the development of IR sensors. In spite of that the studies on the Nd^{3+} emissions in the mid-IR are not frequent [7]. In this study, influence of concentration of RE^{3+} on the photoluminescence of Nd^{3+}-doped $Ga_5Ge_{20}Sb_{10}S_{65}$ glasses is investigated. With the variation of chemical composition in this system, the band-gap can be shifted to lower wavelength which could allow a better pumping at 815 nm required for Nd^{3+} ions. This optical band-gap blue-shift should decrease the optical losses in the pumping spectral range specifically important in the case of fiber use. Thus, in order to blue-shift the optical band-gap, several compositions of the Ga-Ge-Sb-S quaternary system were fabricated and their physicochemical and optical properties have been studied.

The gallium and rare earths combination, their structural environment and resulting interactions, have been assumed to play a fundamental role in the luminescence effectiveness and optical losses of these glass materials and fibers. Thus structural properties have been investigated by Raman spectroscopy, ^{71}Ga NMR and EXAFS at K-edge of Ga, Ge, Sb, S and Nd. Raman spectroscopy is regarded as a standard and non-destructive technique used for chalcogenide glass network analysis; although in the case of a quaternary system not to result in a misleading interpretation is not so straightforward. Whereas ^{71}Ga NMR, rare earths and Ga K-edge EXAFS complementary structural characterizations are much less accessible and only few references are available in the literature [20, 21].

Optical Materials EXPRESS

Moreover, absorption and emission spectra were recorded, fluorescence lifetimes for $^4F_{3/2}$, $^4I_{13/2}$ and $^4I_{11/2}$ energy levels were measured and will be discussed considering spectroscopy parameters obtained by Judd-Ofelt method and structural organization [22, 23].

2. Experimental

2.1 Glass synthesis and physicochemical characterizations

The selected sulfide glass composition for studying the effect of growing introduction of Nd^{3+} is the following: $Ga_5Ge_{20}Sb_{10}S_{65}$ doped with Nd^{3+} ions from 500 to 7500 ppmw. Several other compositions of the Ga-Ge-Sb-S system were also investigated. These glasses were prepared by conventional melting and quenching methods. Ga, Ge, Sb and S elements with high purity (≥ 5N) and neodymium sulfide with 3N purity were used. The commercial sulfur was purified by successive distillations to remove carbon (CO_2, CS_2, COS) and hydrates or sulfides hydrides (H_2O, OH, SH) impurities [24]. Then, chemical reagents were put in silica tubes and pumped under vacuum (10^{-4} mbar). After sealing, the chemical reagents were melted with slow heating to 850°C for 10h in a rocking furnace to ensure homogenization. The ampoule was quenched into water, following by annealing at 290°C for 3h. Single index fibers with 350 µm diameter were obtained by drawing $Ga_5Ge_{20}Sb_{10}S_{65}$ and $Ga_5Ge_{20}Sb_5S_{70}$ preforms of 10 mm diameter and 100 mm length. Bulk glass samples were cut and polished for absorption and fluorescence measurements. Glass transition temperature was determined by using a TA Instrument differential scanning calorimeter DSC 2010, with a heating rate of 10°C/min between room temperature and 450°C. Thermodilatometric analyses were carried out on cylinders of glass approximately 5 mm high in the temperature range of 25 to 250°C by using a thermomechanical analyzer. The measurements were performed at a heating rate of 2 °C/min^{-1} with an applied force of 0.05 N. Density of glass was determined by using a Mettler Toledo XS64. The composition of the different samples was checked by using scanning electron microscopy with an energy-dispersive X-ray analyzer (X Max 80mm^2 Oxford Instruments). The [S-H] content in glasses, which was controlled by the refinement degree of the sulfur purification process, was estimated considering the experimental absorption coefficient from IR-spectra and the extinction coefficient at 4.01 µm (ε = 2.3 dB/m/ppm) [25].

2.2 Optical characterizations

Refractive indices of bulk samples in visible and near-IR were determined by prism coupling technique (Metricon-2010 instrument). A laser beam at several wavelengths (λ = 633, 825, 1064, 1311 and 1551 nm) and a rutile prism were used. Variable angle spectroscopic ellipsometer with rotating compensator (IR-VASE, J. A. Woollam Co., Inc., Lincoln, NE, USA) was employed for the optical characterization of studied materials in ~1.7-15 µm spectral range measuring 50 scans, 15 spectra per revolution at angles of incidence of 50°, 60°, and 70°. To extract optical parameters from VASE data in the 1.7-15 µm spectral region, suitable MIR refractive index spectral dependence function is necessary. In this work, Sellmeier equation in the form $n^2(\lambda) = A + (B\lambda^2/(\lambda^2-C)) + (D\lambda^2/(\lambda^2-E))$, where λ is wavelength, *A, B, C, D*, and *E* are empirical coefficients, was exploited setting extinction coefficient in first approximation to zero [26].

Absorption spectra were measured with Perkin Elmer spectrometer Lambda-1050 in the wavelength range 500-3200 nm and a resolution of 1 nm. Transmission spectra in the IR region were measured with a Bruker Tensor 37 Fourier Transformed Infrared Spectrometer (FTIR) from 2.5 to 15 µm. Fiber attenuation measurements were performed by using the cut-back technique with a Bruker FTIR spectrometer modified with fiber coupling ports [27].

For room-temperature photoluminescence measurements on bulk samples, the pump source was a Ti: Sapphire laser operating at 815 nm. Emission spectra were recorded using an InSb photodiode cooled with liquid nitrogen. The beam was focused on the detector by a

Optical Materials EXPRESS

CaF_2 lens and filters for each emission band. As the spectral response of these detectors is wavelength-dependent, the emission spectra were calibrated by using a tungsten-halogen lamp source and a heat source with emission spectra similar to a black-body source. To record fluorescence signals in the mid-IR spectral region without being perturbed by parasitic absorptions, the monochromator was flushed with dry nitrogen. Fluorescence decays were measured for Nd-doped $Ga_5Ge_{20}Sb_{10}S_{65}$ by using a Nd:YAG-pumped OPO laser at 815 nm delivering 5 ns pulses at 10 Hz with an output energy of ~5 mJ/pulse.

2.3 Structural characterizations

The structure of Ga-Ge-Sb-S glasses was investigated by means of several techniques. The ^{71}Ga NMR experiments have been performed under static conditions at 244.04 MHz with a 18.8 T spectrometer using a 3.2 mm probe-head. The spectra have been recorded using a static 45-τ-45-τ spin echo sequence with 20-50 k accumulations, a recycle delay of 1 s, a full echo delay (2τ) of 400 µs and a 45° pulse length of 1.25 µs. It has been checked that the experimental conditions allowed recording the whole ^{71}Ga NMR signal. The chemical shifts have been referred to $Ga(NO_3)_3$ solution (1 M) at 0 ppm. The Raman spectroscopy was used at ambient temperature on glass samples with an HR800 (Horiba–Jobin-Yvon) unpolarized confocal micro-Raman spectrophotometer with 785 nm laser diode at room temperature using low power density. Reduced Raman intensity of glasses Raman spectra were calculated considering the following equation $I_{red}(\omega) = I(\omega)\omega/[n(\omega) + 1]$ [28, 29]. The term $I(\omega)$ represents the experimental Raman intensity at ω frequency, and $n(\omega)$ is the Bose–Einstein factor, defined as $n(\omega) = (exp[(\hbar\omega/kT)-1])-1$, where $\hbar$ is Planck's constant.

Extended X-ray absorption fine structure (EXAFS) measurements were performed on Nd^{3+}:$Ga_5Ge_{20}Sb_{10}S_{65}$ glasses. EXAFS of powdered glass and bulk were recorded at K-edge of Ga, Ge, Sb, S and Nd at the Italian beamline at ESRF Grenoble. The EXAFS measurements were recorded at room temperature in both, transmission and fluorescence modes. Raw intensities were converted into $\chi(k)$ curves by the Viper program [30]. Coordination numbers, bond lengths and Debye-Waller factors were obtained by fitting the $\chi(k)$ curves with the Viper program. Backscattering and amplitudes and phases needed to calculate the model curves were obtained by the Feff program [31].

3. Results and discussion

3.1 Nd^{3+} doped Ga-Ge-Sb-S bulk glasses characterization

Several compositions were synthetized with an objective of blue-shift of the band-gap by changing the concentration between the different chemical elements. The aim of this shift of the band-gap is to get higher transparency in the visible and near infrared for a better pumping of neodymium ions. Physicochemical properties like glass transition temperature, density, etc. were measured for several compositions from Ga-Ge-Sb-S system.

Table 1. Glass transition temperature, density, Ge/S ratio, stoichiometry deviation R and average coordination number Z for studied compositions

Composition	T_g (± 2°C)	Density (± 0.01g/cm^3)	Ratio Ge/S	R	Z
$Ga_1Ge_{29}Sb_5S_{65}$	372	3.00	0.44	0.96	2.65
$Ga_5Ge_{25}Sb_5S_{65}$	360	3.10	0.38	0.96	2.65
$Ga_1Ge_{24}Sb_5S_{70}$	300	2.89	0.34	1.22	2.55
$Ga_5Ge_{20}Sb_{10}S_{65}$	296	3.21	0.30	1	2.6
$Ga_{10}Ge_{15}Sb_{10}S_{65}$	292	3.26	0.23	1	2.6
$Ga_5Ge_{20}Sb_5S_{70}$	286	2.94	0.28	1.22	2.55
$Ga_5Ge_{15}Sb_{10}S_{70}$	265	3.15	0.21	1.27	2.5

Optical Materials EXPRESS

The average coordination number Z and the stoichiometry deviation R was calculated for each composition. For a glass composition $Ga_wGe_xSb_yS_z$, the average coordination number Z is defined by the Eq. (1):

$$Z = wN_c(Ga) + xN_c(Ge) + yN_c(Sb) + zN_c(S), \quad (1)$$

with $N_c(A)$, the coordination number of atom A; $N_c(Ga) = 4$, $N_c(Ge) = 4$, $N_c(Sb) = 3$ and $N_c(S) = 2$; w, x, y and z, the molar fraction (w + x + y + z = 1).

The R parameter helps to determine the stoichiometry deviation of the chalcogen atoms compare to the other metalloid and metal atoms and is defined in the Eq. (2):

$$R = \frac{zN_c(S)}{wN_c(Ga) + xN_c(Ge) + yN_c(Sb)}. \quad (2)$$

All the data concerning Ga-Ge-Sb-S glasses, glass transition temperature (T_g), density, [Ge/S] ratio, stoichiometry deviation R and average coordination number Z for studied compositions are shown in Table 1.

Concerning temperature of glass transition, we observed that the increase of the [Ge/S] ratio is correlated with an increase of the T_g. We can find in the literature some studies showing the correlation between germanium amount and glass transition temperature of Ge_xS_{1-x} system [32–34]. In these papers, T_g is increasing with the [Ge/S] ratio when it is below 0.5. When the ratio is equal to 0.5, it corresponds to an exact stoichiometry for GeS_2, composed of $[GeS_{4/2}]$ tetrahedra linked mainly by their corners and probably by edges in a lesser extent. This 3D structure producing a highly cross-linked glass network leads to a maximal temperature of glass transition in the binary Ge-S system. In other cases, some weaker (Ge-Ge) or (S-S) homopolar bonds appear that decrease the glass transition temperature. In studied Ga-Ge-Sb-S glasses, all the glasses have a ratio [Ge/S] lower than 0.5 and the T_g is increasing following the ratio, except for the richest one in Ga ($Ga_{10}Ge_{15}Sb_{10}S_{65}$), which presents T_g little bit higher than expected. This anomaly can be explained by its thermal history. We can also notice that, as expected by a previous study, the substitution of gallium for germanium is decreasing the T_g even if both atoms are expected to occupy tetrahedra entities preserving similar cross-linked glass network. The difference in bond energies between Ge-S and Ga-S may explain at least partly T_g changes [35]. The R parameter helps to distinguish over-stoichiometric compositions with more (S-S) bonds and sub-stoichiometric compositions with more (Ge(Ga, Sb)-Ge(Ga, Sb)) or to simplify M-M bonds. Overall, the glass transition temperature increases with the average coordination number Z when R is still around 1, representative of a glass network mainly composed of Ge-S, Ga-S and Sb-S bonds more energetic than M-M bonds.

The expansion coefficient was also measured for studied glasses. A clear tendency appears, with a value of this coefficient around 13-15x10^{-6} K^{-1} for glasses with 65 mol. % of sulfur with R close to 1 (Z = 2.6-2.65) and around 17-18x10^{-6} K^{-1} for glasses with 70 mol. % of sulfur with R close to 1.2-1.3 (Z = 2.5-2.55). The expansion coefficient is clearly lower for higher glass transition temperature. A lower expansion coefficient reflects a higher cross-linked glass network and more energetic bonds.

3.2 Optical properties

Optical band-gap and refractive index for five wavelengths in the visible and near infrared are referenced in Table 2. The Fig. 1 graphically presents the optical band-gap shift for glass compositions studied.

Optical Materials EXPRESS

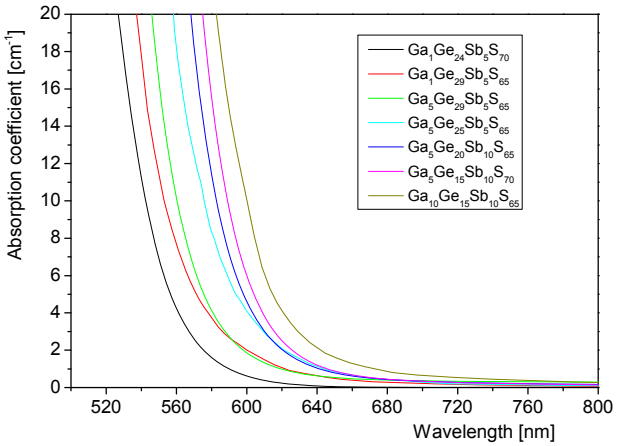

Fig. 1. Absorption coefficient around optical band-gap for several glass compositions.

Concerning the optical band-gap, as expected, a shift is observed with the change of composition. The electronic absorption edge governs the short wavelength limit of the optical transmission window. Chalcogenide glasses are generally considered as amorphous semiconductors with a characteristic optical gap, E_g^{opt}. Incident photons with energy exceeding this gap, $hv > E_g^{opt}$, will excite an electron from the valence to the conduction band creating an electron-hole pair and are absorbed during the process. Recombination of the electron-hole pair occurs in multiple non radiative steps generating phonons rather than photons. The electronic band-gap mainly depends on the electronic configuration and structural arrangement of the atoms in the material. Concerning Ga-Ge-Sb-S glasses, with introducing antimony and gallium elements, there might be an increase of delocalization of nonbonding electrons of sulfur atoms. That could decrease the gap between valence and conduction band and shift the band-gap to longer wavelengths [36]. Consequently, reducing the amount of gallium and antimony leads to the shift of the cut-off wavelength from 601 nm ($Ga_{10}Ge_{15}Sb_{10}S_{65}$) to 542 nm ($Ga_1Ge_{24}Sb_5S_{65}$). The lower electronegativity of gallium, compare to the other elements constituting the glass, rules the band-gap shifting. Four glasses with 5 mol. % of gallium present a shift to lower wavelength; i.e. an increase of their band-gap energy compare to the glass with highest content of gallium (10 mol. %). Considering these four glasses with the same amount of gallium, two glasses with higher content of antimony ($Ga_5Ge_{15}Sb_{10}S_{70}$ and $Ga_5Ge_{20}Sb_{10}S_{65}$) present a really comparable band-gap (589 and 581 nm for the cut-off wavelength, respectively) but also smaller than the two others (560 nm for $Ga_5Ge_{20}Sb_5S_{70}$ and 575 nm for $Ga_5Ge_{25}Sb_5S_{65}$). Keeping gallium and antimony at fixed values, the difference concerns the amount of germanium and sulfur. We could expect that the glass containing more sulfur will have a lower cut-off wavelength compare to the other considering the higher electronegativity of sulfur compare to germanium (χ(S) = 2.58 and χ(Ge) = 2.01). The only glass in contradiction with this rule is the $Ga_5Ge_{15}Sb_{10}S_{70}$ glass for which R coefficient is the highest (R = 1.27) and its band-gap energy is likely affected by the presence of (S-S) bonds in the glass network. The formation of (S-S) bonds, generally expected in case of glass with rich amount of sulfur, will introduce localized levels at the upper part of valence band modifying the electronic structure of the glass and in this specific composition, could decrease the band-gap energy. Finally, glasses with lowest content of gallium (1 mol. %) present a lower band-gap energy with cut-off wavelength of 553 nm for $Ga_1Ge_{29}Sb_5S_{65}$ and of 542 nm for $Ga_1Ge_{24}Sb_5S_{70}$ due to their small content of antimony and gallium.

Optical Materials EXPRESS

Table 2. Overview of some optical properties for several compositions in Ga-Ge-Sb-S system concerning the cut-off wavelength at α = 10 cm^{-1}, refractive index and Abbe number in the 3-5 µm range.

Glass composition	Optical band-gap (nm)	Refractive index (± 5 x 10^{-4})					Abbe number in 3-5 µm range (± 2)
		633 nm	825 nm	1064 nm	1311 nm	1551 nm	
$Ga_{10}Ge_{15}Sb_{10}S_{65}$	601	2.388	2.325	2.294	2.279	2.271	126
$Ga_5Ge_{15}Sb_{10}S_{70}$	589	2.373	2.308	2.277	2.262	2.254	147
$Ga_5Ge_{20}Sb_{10}S_{65}$	581	2.368	2.302	2.272	2.258	2.251	155
$Ga_5Ge_{25}Sb_5S_{65}$	575	2.284	2.234	2.208	2.196	2.189	197
$Ga_5Ge_{20}Sb_5S_{70}$	560	2.254	2.205	2.180	2.168	2.161	164
$Ga_1Ge_{29}Sb_5S_{65}$	553	2.239	2.192	2.169	2.157	2.151	216
$Ga_1Ge_{24}Sb_5S_{70}$	542	2.233	2.180	2.155	2.145	2.139	198

Comprehensively, the low content of gallium and antimony in sulfide glasses rule the band-gap shift to lower cut-off wavelength. To increase the content of sulfur in these glasses is generally also a good way to shift the band-gap to lower wavelength.

Antimony and gallium are also involved in the change of the refractive index for Ga-Ge-Sb-S glasses (Table 2, Fig. 2). Firstly, the glasses containing 10 mol. % of antimony have higher refractive index than other glasses with 5 mol. % of antimony. The antimony is known for clearly increase of the refractive index [37]. Secondly the refractive index increases with the content of gallium inside our glasses. For example, at 1551 nm (far from the absorbing spectral range), the glass $Ga_1Ge_{24}Sb_5S_{70}$, with 1 mol. % of gallium, has a refractive index about 2.139 while the glass $Ga_5Ge_{20}Sb_5S_{70}$, with 5 mol. % of gallium, has a refractive index about 2.161. At 1551 nm, the contrast of refractive index (Δn) ranging from 0.022 to 0.04 can be obtained by substituting gallium for germanium atoms of about 5-10 mol. % in good agreement with Troles *et al.* [35]. The contrast Δn is slightly lower and ranging from 0.003 to 0.028 by substituting sulfur for germanium atoms of about 5 mol. % depending on composition. Finally, the contrast Δn is the highest by substituting antimony for germanium or antimony for sulfur of 5 mol. % with maximum Δn of 0.09. Antimony possesses a highly polarizing effect, related to its electronic density and ionic radius, higher than the other elements contained in the glass. Regarding the glass density, it can be emphasizing the classical almost linear increase of the refractive index with the density [38]. We can easily understand the predominant role of antimony. Therefore, antimony and to a lesser extent gallium have an important influence on refractive index of studied glasses.

Another way to determine refractive index, especially in mid-infrared, is to use ellipsometry showing the normal dispersion of the refractive index from near- to mid-infrared spectral range (Fig. 2). Optical dispersion has been evaluated in the 3-5 µm range by using the modified Abbe number as follows:

$$V_{3-5} = \frac{n_4 - 1}{n_3 - n_5}, \tag{3}$$

where $V_{3\text{-}5}$ is the Abbe number for the 3-5 µm atmospheric windowand n_x is the refractive index at different wavelengths (in µm). The results are shown in Table 2. A higher Abbe number means a lower chromatic dispersion. Globally, the Abbe number decreases when the content of germanium decreases and the content of gallium increases.

Optical Materials EXPRESS

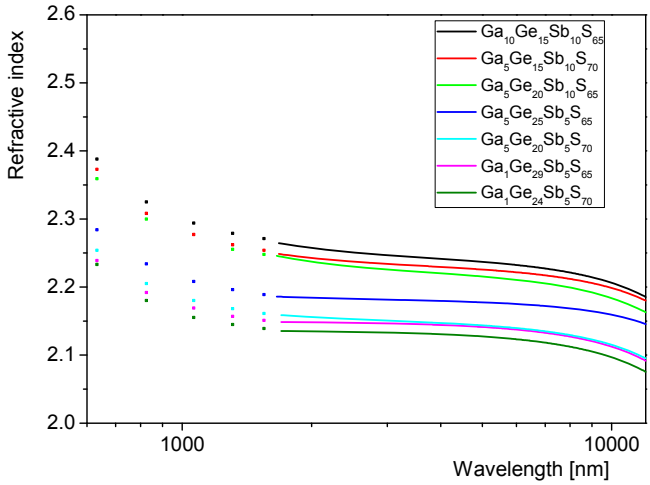

Fig. 2. Refractive index obtained by prism coupling (dots) and ellipsometry (line) for several compositions of Ga-Ge-Sb-S system.

From these optical measurements results, one composition was selected due to the interesting shift of the cut-off wavelength to lower wavelength (560 nm versus 581 nm for $Ga_5Ge_{20}Sb_{10}S_{65}$ glass) and also the thermo-mechanical properties suitable for a fiber drawing. This composition, $Ga_5Ge_{20}Sb_5S_{70}$ has been used for spectroscopic comparison to $Ga_5Ge_{20}Sb_{10}S_{65}$ glass.

3.3 Structural characterization of glasses from Ga-Ge-Sb-S quaternary system

The Ge-S glass system is known to be mainly formed by [$GeS_{4/2}$] tetrahedra linked by their corners and also partly by edges in the case of stoichiometric glass GeS_2. For sulfur deficient glasses, the germanium atoms can be linked by Ge-Ge homopolar bonds forming $GeS_{4-x}Ge_x$ (x = 1, 2, 3 or 4) or S_3Ge-GeS_3 ethane-like structural units. For sulfur rich glasses, tetrahedra are linked each other by sulfur dimers or short chains and even rings, generating (S-S) bonds [39]. Ga-Ge-Sb-S system comes from the two ternary Ge-Sb-S and Ge-Ga-S systems well described in literature. The Ge-Sb-S system is formed by [$GeS_{4/2}$] tetrahedra linked by their corners and edges equivalent to what can be observed in the Ge-S binary system and presenting also (S-S) bonds for compositions with an excess of sulfur, according to Raman spectroscopy [40], and (Ge(Sb)-(Sb)Ge) bonds for sulfur deficient glasses. Only Sb^{3+} species seem to exist in this Ge-Sb-S matrix and can form [$SbS_{3/2}$] pyramidal units [40, 41]. Considering Ge-Ga-S system, the glass network is constituted of [$GeS_{4/2}$] and [$GaS_{4/2}$] tetrahedra linked by corners and edges, according to X-ray absorption spectroscopy [42, 43]. Revealed by Raman scattering spectroscopy, ($S_3Ge(Ga)$-$(Ga)GeS_3$) units are proposed to exist [44, 45]. The aim of this study is to better describe the glass network based on Ga-Ge-Sb-S system by means of ^{71}Ga NMR, Raman spectroscopy and EXAFS.

Concerning ^{71}Ga NMR, spectra given in Fig. 3(a) have been recorded for several compositions. Some NMR spectra of crystallized samples, like $BaGa_2S_4$ and $CaGa_2S_4$ both well-known for rare earth doping [46, 47], GaS or Ga_2S_3 and glass-ceramics such as $Ga_{12.5}Ge_{12.5}Sb_{10}S_{65}$ and $Ga_{15}Ge_{10}Sb_{10}S_{65}$ are proposed to compare the signal of known structures with our glasses (Fig. 3(b)).

Optical Materials EXPRESS

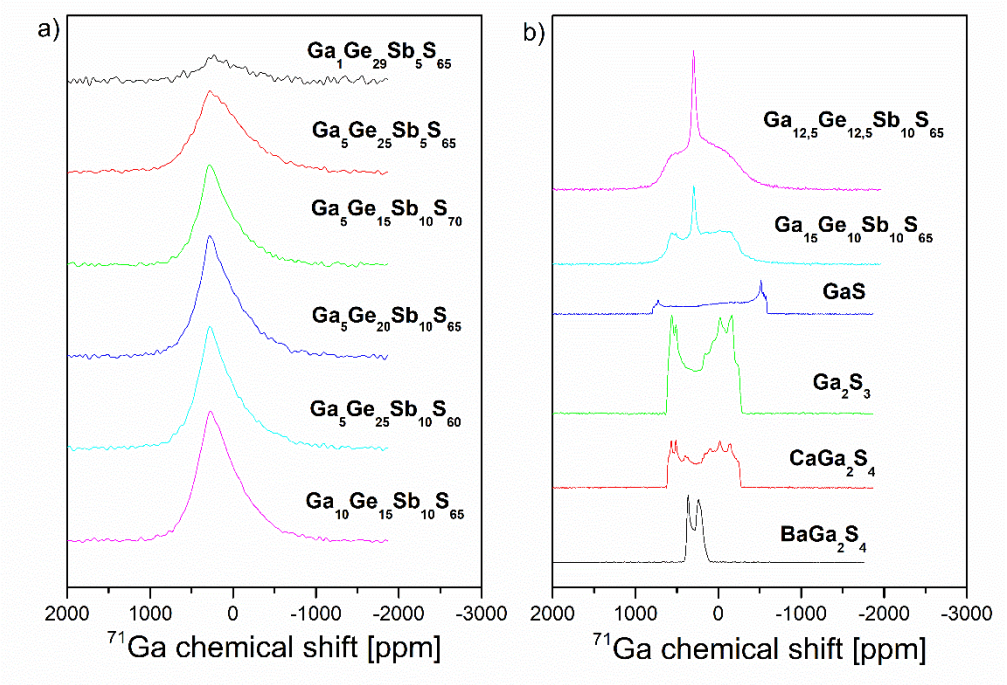

Fig. 3. ^{71}Ga NMR spectra for glasses of the Ga-Ge-Sb-S system (a) and for some glass-ceramics and crystals (b).

First, when considering the whole spectrum, the line shape looks strongly structured by the quadrupolar interaction for both the glasses and the crystals. The shape observed for $BaGa_2S_4$ is characteristic of single environment for gallium, in agreement to its structure indicating only one crystallographic site. This crystal is composed of tridimensional [GaS_4] tetrahedra connected by their corners [21, 48, 49]. The small line width is in agreement with the high symmetry of the crystal. For $CaGa_2S_4$, Ga_2S_3 and GaS, their line shapes are much larger and result from an overlap of several contributions (two at least). Effectively, $CaGa_2S_4$ presents two crystallographic sites for the gallium, with tetrahedron arrangement in layers corresponding to a 2D structure. These tetrahedra are linked by their corners and also by their edges forming dimers. In that case, sulfur is coordinated by two or three atoms of gallium. Its spectrum shows more than two contributions and could be attributed to parasites due to pollution by oxides. The line shape of Ga_2S_3 spectra is very close to the previous one observed, $CaGa_2S_4$. The most common variety of Ga_2S_3 presents also two Ga crystallographic sites and it is generally described as a 3D network of tetrahedra linked only by their corners but where sulfur can be three-fold coordinated. The local symmetry around gallium is also very similar to $CaGa_2S_4$. Layer structuration is probably the reason why the two spectra are very similar, even if it happens to find three Ga crystallographic sites, especially in α-Ga_2S_3 phase. Concerning GaS, a particular shape can be observed showing good crystallization and quadrupolar interaction in axial symmetry. It is common to observe this axial symmetry as the environment of gallium is strongly conditioned by the unidirectional Ga-Ga bond. Moreover, the line shape is significantly larger than previous ones, and particularly than the line shape observed for glasses consequent to a distribution of quadrupolar parameters. From these observations, we can conclude that quadrupolar parameters specific to an environment associated to homopolar bonds were not found even if they are expected in low proportions.

The two last spectra of Fig. 3(b) concern glass-ceramics, with an amorphous phase and crystallized phases. The amorphous and crystalline components are well defined in each NMR spectrum, with a large structured contribution and a fine contribution in the center. The

Optical Materials EXPRESS

large contribution of the spectrum was attributed to Ga crystallized phase, which could seem paradoxical. The line shape looks like the other line shapes observed for previous crystals, $BaGa_2S_4$ and Ga_2S_3. It is necessary to remind that for quadrupolar nuclei like ^{71}Ga, the line shape width corresponds to the site symmetry and not to the structural disorder. The fine contribution that emerges in the center corresponds in fact to gallium in crystallographic sites of high symmetry, typically cubic sites. It is very common to find this situation in amorphous materials in which quadrupolar parameters are distributed by local disorder corresponding to high symmetry situations. The largest part of the line shape, corresponding to low symmetry sites, is hidden through the crystalline phase contribution.

Line shapes coming from continuous distribution of quadrupolar parameters are observed in Fig. 3a. This line shape is very common and systematically observed for highly quadrupolar nuclei as ^{71}Ga, ^{27}Al, ^{23}Na, for example, in glasses. For this type of materials, the expected distribution of quadrupolar parameters has been determined by Czjzek [20]. Line shapes observed here perfectly matches these distributions. Very little changes were observed between spectra of investigated glasses. Widths and positions are the same as those observed in crystals and glass-ceramics. This confirms that in these amorphous materials, gallium is coordinated with four sulfur atoms forming GaS_4 tetrahedra. Moreover, for compositions containing less sulfur, no signature of Ga-Ga homopolar bond is clearly observed. This information is important for discussion concerning Raman spectra analysis. Finally, it can be noted that spectrum of 5% antimony glass is slightly wider than the others, showing the higher disorder of gallium environment. It is in agreement with the important role of antimony for the glass forming.

Several compositions studied in this paper have been investigated with Raman spectroscopy (Fig. 4(a), Tab. 3). The Raman spectra of Ga-Ge-Sb-S glasses are dominated by the presence of the band peaking at 340 cm^{-1} related to the $\nu_1(A_1)$ symmetric stretching modes of tetrahedral [$GeS_{4/2}$] [50] as it can be seen for illustration in Fig. 4(b). A shoulder is observed at 370 cm^{-1}, corresponding to a companion mode of the ν_1 mode linked to vibrations of tetrahedra bound by their edges [51]. A widening of the dominant peak is visible for composition with high amount of gallium (10%) attributed to symmetric stretching mode of [$GaS_{4/2}$] tetrahedra, around 320 cm^{-1}. A shoulder located at 296 cm^{-1} is attributed to the symmetric stretching vibration modes of [$SbS_{3/2}$] pyramids [52]. In the Raman spectra corresponding to glasses with an excess of sulfur (typically compositions with 70% of sulfur), we observe two bands located at 474 and 218 cm^{-1} (Fig. 4(c)). These bands are attributed to the stretching and bending vibrations mode of S-S homopolar bonds, respectively which can form dimers, small chains or S_8 rings [51]. A small peak at 152 cm^{-1} could be assigned to the Sb-Sb bonds vibrations [53, 54] but are more probably due to the presence of S_8 rings, the main vibration bands of which are centered at 151, 218 and 476 cm^{-1} [55]. Moreover, in the Fig. 4(d), a weak band is observed at 258 cm^{-1}. This band can be associated to vibrations modes of Ge-Ge homopolar bonds (usually at 250-258 cm^{-1}), existing in $S_3Ge\text{-}GeS_3$ units [41]. It can be also Ga-Ge(Ga) bonds (expected around 268 cm^{-1} for Ga-Ga(Ge)) but it is quite difficult to distinguish them due to their very close atomic weight. Fortunately, ^{71}Ga NMR gives information about gallium bonds and shows that there are no homopolar Ga-Ga bonds. A weak band observed at 205 cm^{-1} could be attributed to the presence of clusters $SGe_3\text{-}S_{6/3}$ presents in GeS_2 [56] or likely to the presence of Ge-Sb bonds [57]. A band at 430 cm^{-1} is assigned to the vibrations of $S_3Ge\text{-}S\text{-}GeS_3$ units where the tetrahedra are connected by their corners.

Optical Materials EXPRESS

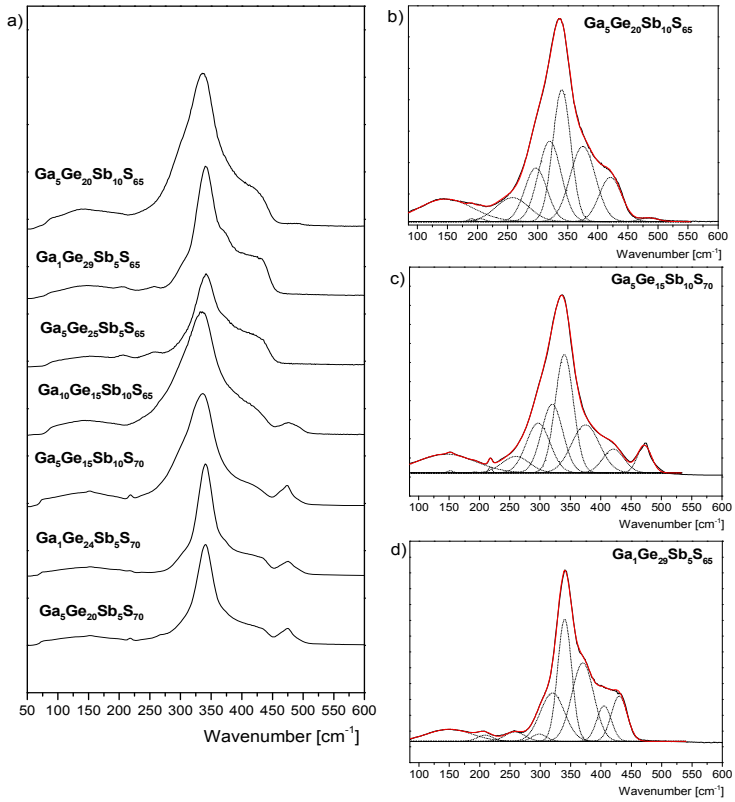

Fig. 4. Raman spectra of several glass compositions of Ga-Ge-Sb-S system (a), deconvoluted Raman spectrum of $Ga_5Ge_{20}Sb_{10}S_{65}$ (b), $Ga_5Ge_{15}Sb_{10}S_{70}$ (c) and $Ga_1Ge_{29}Sb_5S_{65}$ (d).

Table 3. Characteristic vibration mode observed in Ga-Ge-Sb-S system by Raman spectroscopy

Wavenumber	**Signal**	**Attribution**	**References**
145-150 cm^{-1}	large band	distortion mode of [$GeS_{4/2}$] tetrahedra	[58]
152 cm^{-1}	band	vibration mode of homopolar Sb-Sb bond	[53,54]
190 cm^{-1}	band	bending vibration mode of S-S bonds in S_8 rings	[51]
205 cm^{-1}	weak band	vibration mode of presence of Ge-Sb bonds or Ge-S bond in SGe_3-$S_{6/3}$ cluster	[57] [56]
218 cm^{-1}	band	bending vibration mode of S-S bonds in S_8 rings	[59]
258 cm^{-1}	weak band	stretching mode of Ge-Ge homopolar bonds	[41]
296 cm^{-1}	shoulder	symmetric stretching mode of [$SbS_{3/2}$] pyramid units	[52]
320 cm^{-1}	shoulder	symmetric stretching mode of [$GaS_{4/2}$] tetrahedra	[52]
340 cm^{-1}	band	symmetric stretching mode ν_1 (A_1) of [$GeS_{4/2}$] tetrahedra	[50]
370-375 cm^{-1}	shoulder	companion mode (A_c), vibration mode of Ge-S bond for [$GeS_{4/2}$] tetrahedra linked by edge	[51]
405 cm^{-1}	band	asymmetric bending mode of [$GeS_{4/2}$] tetrahedra	[50]
425-430 cm^{-1}	band	vibration mode of S_3Ge-S-GeS_3 units with [$GeS_{4/2}$] tetrahedra linked by their corner	[60]
474 cm^{-1}	weak band	vibration mode of S-S homopolar bonds	[51]

The Fig. 5 presents EXAFS spectra and radial distribution function not corrected by the phase shift. The results (Table 4) show that the gallium is surrounded by 4.10 sulfur atoms with a Ga-S bond distance of 2.28 Å. Higuchi *et al.* obtained similar results for Ga_2S_3-GeS_2-

Optical Materials EXPRESS

La_2S_3 system with a Ga-S bond distance of 2.31 Å and Ga coordination number of 4.2 [58]. Information confirm conclusion of Raman spectroscopy and NMR: these glasses are constituted by GaS_4 tetrahedra. The value obtained by EXAFS is in good agreement with the bond valence sum (BVS) [59]. This theory predicts for a $[GaS_{4/2}]$ tetrahedron, a Ga-S bond distance of 2.27 Å and a coordination number equal to 4.12.

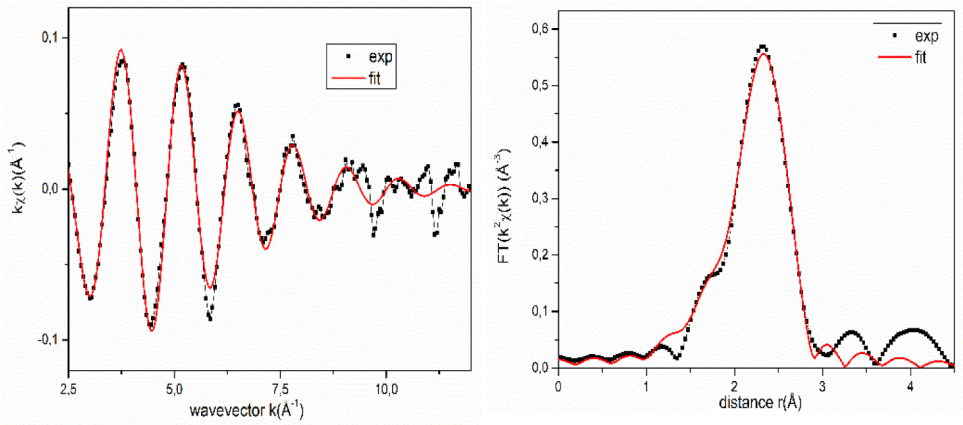

Fig. 5. EXAFS spectrum showing oscillations (left) and radial distribution function non-corrected of phase shift (right) for Nd^{3+} ions in $Ga_5Ge_{20}Sb_{10}S_{65}$ glass.

The germanium is surrounded by 4.14 sulfur atoms with a Ge-S bond distance of 2.23 Å. These results confirm the four-coordination of germanium and the presence of $[GeS_{4/2}]$ tetrahedra. The values are close to values from the literature (Ge-S = 2.21 Å with a coordination number of 4.2 for Ga_2S_3-GeS_2-La_2S_3 system [58]) and in good agreement with a Ge-S bond distance of 2.23 Å and a coordination number (N_c = 4.14) predicted with the BVS for a $[GeS_{4/2}]$ tetrahedron.

The antimony is surrounded by 3.0 sulfur atoms with a Sb-S bond distance of 2.47 Å. The good agreement with the BVS (2.47 Å and N_c = 2.97 for SbS_3) is in line with the presence of $[SbS_{3/2}]$ pyramids units. Nevertheless, the value of bond distance is different from several studies giving a Sb-S bond distance of 2.34 Å.

The neodymium is surrounded by 10.83 sulfur atoms and the Nd-S bond distance is about 2.95 Å. The literature is very poor concerning data on local structure of Nd in sulfide glasses. However, coordination of neodymium seems to be overrated if we refer to estimations of BVS (N_c = 8.63 and Nd-S = 3.03 Å). One reason of this overrating could be due to the quality of the recorded data. The dilution of neodymium in the matrix and the difficulty to work at high energy are two problems leading to such low quality. In general, coordination number is the most affected parameter when the data are not presenting a high-quality.

Table 4. Coordination numbers (N), bond distances (R) and Debye-Waller factors (σ^2) of Ga-S, Ge-S, Sb-S, and Nd-S bonds in $Ga_5Ge_{20}Sb_{10}S_{65}$ glass, with R-factor showing the validity of fitting

Bond	N	N_{calc}	R (Å)	R_{calc} (Å)	σ^2 (Å^2)	R-factor
Ga-S	4.10	4	2.28 (0.01)	2.27	0.0077 (0.002)	0.014
Ge-S	4.14	4	2.23 (0.01)	2.22	0.0034 (0.001)	0.004
Sb-S	2.97	3	2.47 (0.01)	2.47	0.0051 (0.001)	0.008
Nd-S	10.83	8.63	2.95 (0.01)	3.03	0.0121 (0.002)	0.008

R-factor measures the misfit relative to the data

Optical Materials EXPRESS

The different methods used for structural characterization give us information about the glass network organization of some Ga-Ge-Sb-S host matrices. These glass matrices are composed of [$GaS_{4/2}$] and [$GeS_{4/2}$] tetrahedra with probably weak proportion of Ge-Ge, Ge-Sb bonds but not Ga-Ga bonds. These Ge-Ge(Sb) bonds can form S_3Ge-Ge(Sb)S_3 units. [$SbS_{3/2}$] pyramids units are also present with maybe few Sb-Sb bonds for rich antimony glasses. It cannot be absolutely excluded that antimony is present in higher coordination like SbS_4 or SbS_5 entities. Some clues suggest that further study is needed to investigate this hypothesis. S-S bonds forming chains and S_8 rings have been observed for Ga-Ge-Sb-S glasses with an excess of sulfur. Concerning the rare earth, neodymium was found to be surrounded by 10.8 sulfur atoms. This coordination is probably overrated compared to other rare earth already studied in sulfide matrix as the Nd^{3+} ionic radius, that is about 2.95 Å, is relatively close to these other rare earths [52, 61].

3.4 Spectroscopy of Nd^{3+} in $Ga_5Ge_{20}Sb_{10}S_{65}$ and $Ga_5Ge_{20}Sb_5S_{70}$ glass

The study was carried out on bulk glasses with the selected composition $Ga_5Ge_{20}Sb_{10}S_{65}$ (thereinafter 2S2G) doped with different neodymium concentrations (500, 2400, 3900, 5000 and 7500 ppmw.). Several dopant concentrations were tested to investigate the energy transfer rates between neighboring ions, which could lead to the quenching of the luminescence. In the absorption spectra, the intensities of Nd^{3+} absorption bands increase linearly with the Nd^{3+} concentration (Fig. 6).

Considering a pumping at 814 nm (Fig. 7), the near-IR transitions arise mainly from the $^4F_{3/2}$ emitting manifold, while the mid-IR transitions (wavelength longer than 2 µm), arise only from the lower ^4I_J manifolds.

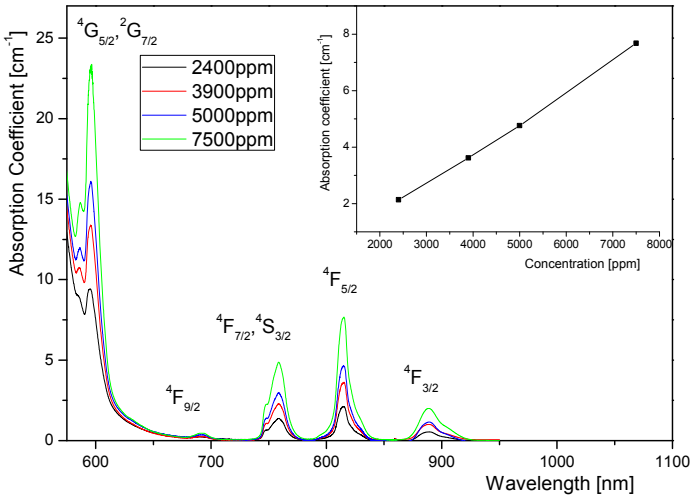

Fig. 6. Evolution of absorption coefficient for several Nd^{3+} concentrations in 2S2G glass, with the inset showing the absorption coefficient for the $^4F_{5/2}$ level.

Judd-Ofelt (JO) calculations and spectroscopic characterization have been done within $Ga_5Ge_{20}Sb_{10}S_{65}$ (2S2G) and the other composition selected, $Ga_5Ge_{20}Sb_5S_{70}$ (GaGeSbS-S70). Eight absorption bands of Nd^{3+} ions, shown in Fig. 8 for $Ga_5Ge_{20}Sb_{10}S_{65}$ (2S2G) and GaGeSbS-S70, corresponding to $^4I_{9/2} \rightarrow {}^4G_{5/2} + {}^2G_{7/2}$, $^4I_{9/2} \rightarrow {}^4F_{9/2}$, $^4I_{9/2} \rightarrow {}^4F_{7/2} + {}^4S_{3/2}$, $^4I_{9/2} \rightarrow {}^4F_{5/2} + {}^2H_{9/2}$, $^4I_{9/2} \rightarrow {}^4F_{3/2}$, $^4I_{9/2} \rightarrow {}^4I_{15/2}$, $^4I_{9/2} \rightarrow {}^4I_{13/2}$ and $^4I_{9/2} \rightarrow {}^4I_{11/2}$ transitions can be observed at 595, 691, 757, 813, 893, 1572 to 1798, 2316 to 2794 and 4397 to 6321 nm respectively. Energy diagram was also determined from experimental data as presented in Fig. 7.

Optical Materials EXPRESS

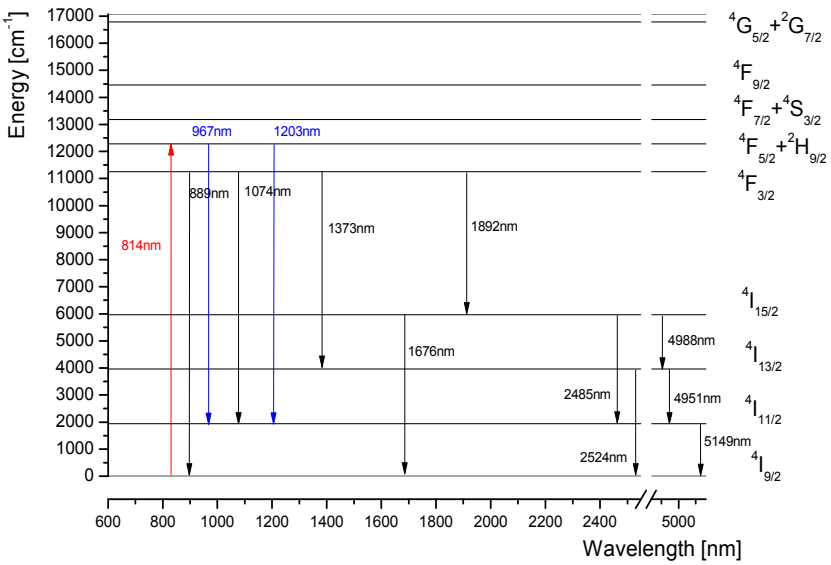

Fig. 7. Energy diagram of Nd^{3+} ion in 2S2G glass matrix.

Intensities of absorption bands of Nd^{3+} ions increase with the concentration of Nd^{3+}. In the Fig. 6, the evolution of the absorption coefficient at a given wavelength depending on the concentration is shown. This change of absorption coefficient is linear with the concentration of rare earth and provides to check easily the real concentration for other samples. It can be noted that absorption cross section is not changing with increasing the rare earth concentration. In oxides matrices, absorption cross-section for the transition $^4I_{9/2} \rightarrow {}^4F_{5/2} + {}^2H_{9/2}$ is $2.5x10^{-20}$ cm^2 [62]. In Ga-La-S sulfide matrices, absorption cross-section for the same transition is $3.79x10^{-20}$ cm^2 [63]. In comparison, the absorption cross-section, which is about $7.2x10^{-20}$ cm^2 in $Ga_5Ge_{20}Sb_{10}S_{65}$ (2S2G) and $7.7x10^{-20}$ cm^2 in $Ga_5Ge_{20}Sb_5S_{70}$ (GaGeSbS-S70), is higher in our host glass matrices, moreover exhibiting a lower phonon energy than oxides or Ga-La-S matrices. Nevertheless, it must be noticed that for $20GaS_{3/2}$-$50GeS_2$-$30SbS_{3/2}$-$3NdS_{3/2}$ glass, a lower value of about $2.2x10^{-20}$ cm^2 [7] was recorded. Using the integrated absorption cross-sections, a Judd-Ofelt analysis had been performed to estimate the radiative lifetimes and the branching ratios for the infrared transitions. Using the matrix elements from Carnall et al. [64], a standard calculation has been used for determining the phenomenological Judd-Ofelt parameters: $\Omega_2 = 9.2\ x10^{-20}$; $\Omega_4 = 9.1\ x10^{-20}$; $\Omega_6 = 4.7\ x10^{-20}$ for 2S2G and $\Omega_2 = 6.9\ x10^{-20}$; $\Omega_4 = 11.7\ x10^{-20}$; $\Omega_6 = 4.4\ x10^{-20}$ for GaGeSbS-S70. The value of Ω_2 parameter is relatively similar to those for other sulfide glasses and other rare earth [7, 65]. It is known that Ω_2 is affected by the local symmetry of ligand field or covalency of chemical bond between rare earth and ligand atoms; $\Omega_{2\ sulfide} > \Omega_{2\ oxide} > \Omega_{2\ fluoride}$ [66]. The sulfur richest composition of the glass matrix seems to affect the symmetry of the Nd^{3+} or likely could decrease its chemical bond covalency. The compositional variation of Ω_6 is expected to present an opposite tendency to a lesser extent. The results presented in Table 5 and 6 for 2S2G and GaGeSbS-S70, respectively, only concern the cascade transitions occurring after a 815 nm optical pumping ($^4I_{9/2} \rightarrow {}^3F_{5/2}$), which correspond to the highest absorption cross-section of the pump.

Optical Materials EXPRESS

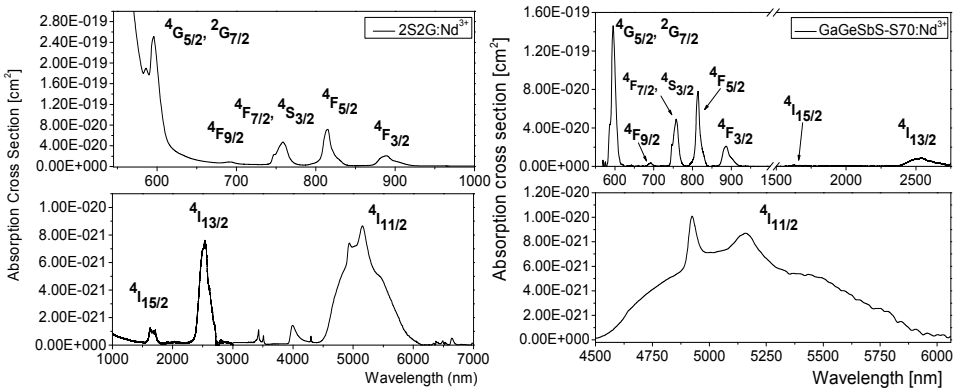

Fig. 8. Absorption cross-section of Nd-doped 2S2G glass (a) and Nd-doped GaGeSbS-S70 glass (b).

Table 5. Radiative parameters of Nd^{3+} ions in 2S2G glass calculated using Judd-Ofelt analysis.

transition		λ (nm)	ΔE (cm^{-1})	β (%)	τ (μs)
$^4I_{11/2}$	$^4I_{9/2}$	5208	1920	100	26424
$^4I_{13/2}$	$^4I_{11/2}$	4943	2023	33	7654
	$^4I_{9/2}$	2536	3943	67	
$^4I_{15/2}$	$^4I_{13/2}$	4908	2038	28	6978
	$^4I_{11/2}$	2463	4061	54	
	$^4I_{9/2}$	1672	5981	18	
$^4F_{3/2}$	$^4I_{15/2}$	1917	5217	0	70
	$^4I_{13/2}$	1378	7255	6	
	$^4I_{11/2}$	1078	9278	39	
	$^4I_{9/2}$	893	11198	55	
$^4F_{5/2}$, $^2H_{9/2}$	$^4F_{3/2}$	9740	1027	0	59
	$^4I_{15/2}$	1602	6244	5	
	$^4I_{13/2}$	1207	8282	17	
	$^4I_{11/2}$	970	10305	14	
	$^4I_{9/2}$	818	12225	63	

For 2S2G and GaGeSbS-S70 sulfide glass, the average phonon energy can be estimated from Raman spectroscopy about 340 cm^{-1}. Considering that for transitions energies exceeding five times the phonon energy, the radiative decay is quenched, so that the $^4F_{5/2}$ pumping is leading to an efficient population of the $^4F_{3/2}$ manifold, from the small 1027 cm^{-1} energy gap. The non-radiative transfer is not excluding some radiative transitions in the near-IR spectral range (Fig. 9 inset). Considering the $^4F_{3/2}$ emitting manifold, only radiative transitions can occur, as the energy gap is higher than 5000 cm^{-1}. The measured luminescence properties are reported in Fig. 9. From this spectrum, the emission intensities could be integrated for the experimental branching ratios determination, following Eq. (4):

$$\beta_{ji} = \frac{I_{ji} \times \lambda_{ji}}{\sum_k I_{jk} \times \lambda_{jk}}, \tag{4}$$

where *j* and *i* are respectively the upper and the lower manifold.

Optical Materials EXPRESS

In recorded spectra, the $^4F_{3/2} \rightarrow {}^4I_{9/2}$ emission is strongly affected the radiation reabsorption, explaining the difference between the calculated and measured $^4F_{3/2} \rightarrow {}^4I_{9/2}$ branching ratio. These experiments have been performed on bulk glasses, so that that this zero-line phonon radiation could be reabsorbed on the optical path, resulting in an experimental $^4I_{11/2}$ branching ratio lower than the Judd-Ofelt calculations, and thus making the remaining experimental branching ratios ($^4I_{11/2}$, $^4I_{13/2}$ and $^4I_{15/2}$) higher than the calculated ones, but confirming the rate between the $^4I_{13/2}$ and $^4I_{11/2}$.

Table 6. Radiative parameters of Nd^{3+} ions in GaGeSbS-S70 glass calculated using Judd-Ofelt analysis.

transition		λ (nm)	ΔE (cm^{-1})	β (%)	τ (μs)
$^4I_{11/2}$	$^4I_{9/2}$	5190	1927	100	31039
$^4I_{13/2}$	$^4I_{11/2}$	5052	1979	33	9669
	$^4I_{9/2}$	2560	3906	67	
$^4I_{15/2}$	$^4I_{13/2}$	4845	2064	30	8520
	$^4I_{11/2}$	2473	4044	52	
	$^4I_{9/2}$	1675	5970	18	
$^4F_{3/2}$	$^4I_{15/2}$	1885	5305	0	69
	$^4I_{13/2}$	1357	7273	5	
	$^4I_{11/2}$	1070	9346	35	
	$^4I_{9/2}$	887	11274	60	
$^4F_{5/2}$, $^2H_{9/2}$	$^4F_{3/2}$	9890	1011	0	61
	$^4I_{15/2}$	1583	6317	6	
	$^4I_{13/2}$	1193	8382	17	
	$^4I_{11/2}$	965	10363	15	
	$^4I_{9/2}$	814	12285	62	

The emission spectra were obtained by pumping the samples at 815 nm ($^4F_{5/2}$ and $^2H_{9/2}$ levels) to populate $^4F_{3/2}$ level. This wavelength provides an efficient absorption (Fig. 8). Fig. 9 shows the emission spectra of Nd^{3+}-doped samples with several concentrations. Here, the bands are corresponding to transitions from $^4F_{3/2}$ to the lower $^4I_{9/2}$, $^4I_{11/2}$ and $^4I_{13/2}$ levels. The $^4F_{3/2} \rightarrow {}^4I_{9/2}$ emission, at 915 nm, is very interesting to be transmitted by a classical silica fiber. The neodymium presents an absorption band around 5 μm. The emission of the praseodymium could be absorbed by the neodymium, reemitted at 915 nm and then transmitted by a classical silica fiber. It could open new way to detect molecules absorbing in mid-IR with a full optic sensor [67].

Although the $^4F_{3/2}$ emissions are clearly attributed (1.4 and 2.0 μm), the 2.5 μm emission band should be discussed. The energy levels display of the four ^4I_J levels can lead to potentially three distinctive 5 μm emissions lines, and two at the wavelength of 2.5 μm (Fig. 7). As the $^4I_{15/2} \rightarrow {}^4I_{9/2}$ line could be observed at 1550 nm and considering the Judd Ofelt calculations, the $^4I_{15/2} \rightarrow {}^4I_{11/2}$ line will also be observed at 2.5 μm. This band results mainly from the $^4I_{13/2} \rightarrow {}^4I_{9/2}$ fluorescence, but the $^4I_{15/2} \rightarrow {}^4I_{11/2}$ contribution could be estimated to be roughly six times lower, from (JO – branching ratio) Table 5 and 6. For the 5 μm emission, three radiative schemes are possible, but the $^4I_{11/2} \rightarrow {}^4I_{9/2}$ line brings the strongest contribution, by more than one order of magnitude, based on the branching ratios calculations. Assuming that the observed fluorescence is due to the $^4I_{11/2} \rightarrow {}^4I_{9/2}$ emission, this emission band could be cross-section calibrated using the Füchtbauer-Ladenburg formula (Eq. (5)):

Optical Materials EXPRESS

$$\sigma_e(\lambda) = \frac{\lambda^5}{8\pi c \cdot n^2} \cdot \frac{\beta}{\tau} \cdot \frac{i(\lambda)}{\int_{ij} \cdot \lambda \cdot i(\lambda) d\lambda} \quad (5).$$

The integration is performed on the full transition bandwidth, denoted *ij*.

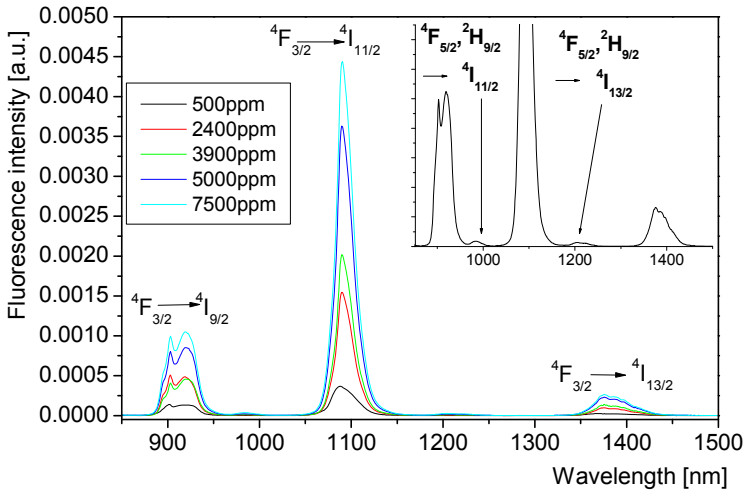

Fig. 9. Emission spectra of Nd^{3+} doped 2S2G glass with different concentrations of rare earth.

The $^4F_{3/2}$ emission cross-section calculations are reported in Table 7. Usually, the calibration is calculated using the predicted β and τ from the Judd-Ofelt calculations. Here, most of the expected transitions fluorescence signals and radiative lifetimes were recorded, so that the cross-section could be calculated for 2S2G glass. Emission cross section are quite higher compare to Ga-Ge-S-CsCl system which is about $0.5x10^{-20}$ cm^2 for the $^4F_{3/2} \rightarrow {}^4I_{13/2}$ transition [68], and a bit lower compare to Zn-Bi borate system ($4x10^{-20}$ cm^2) for the $^4F_{3/2} \rightarrow {}^4I_{11/2}$ transition [69].

Table 7. Experimental and calculated $^4F_{3/2}$ branching ratios and emission cross-sections for 2S2G and 2S2G-S70

final level	λ (nm)	2S2G			2S2G-S70		
		β (exp)	β (JO)	Emission cross-section [cm^2]	β (exp)	β (JO)	Emission cross-section [cm^2]
$^4I_{9/2}$	916	0.21	0.55	$1.2 x10^{-20}$	-	-	-
$^4I_{11/2}$	1095	0.67	0.39	$1.3 x10^{-19}$	-	-	-
$^4I_{13/2}$	1387	0.1	0.06	$2.6 x10^{-20}$	0.08	0.05	$1.82 x10^{-20}$
$^4I_{15/2}$	1982	0.02	0	$7.2 x10^{-21}$	-	-	-

With pulsed excitation of the $^4I_{11/2}$, $^4I_{13/2}$ and $^4F_{3/2}$, respective fluorescence decay curves at 5, 2.6 and 1.3 μm were recorded (Fig. 10).

Optical Materials EXPRESS

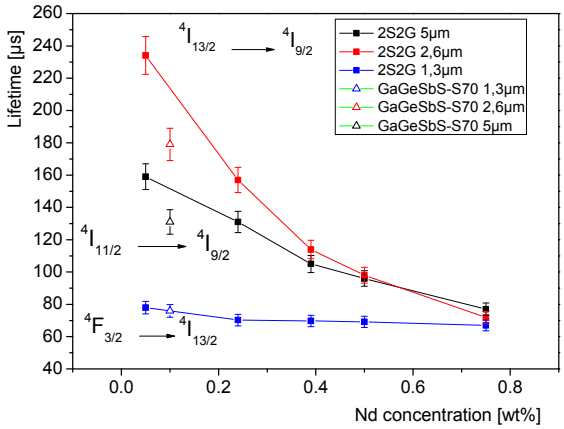

Fig. 10. Fluorescence lifetimes measured for Nd^{3+} ions in 2S2G and GaGeSbS-S70 glasses.

For these levels, lifetimes were determined by an exponential fit of the fluorescence decay curves. The fluorescence lifetime of the $^4F_{3/2}$ level, for the lowest Nd^{3+} concentration, is found very close to the Judd-Ofelt prediction 70 µs (Table 5,6). For the ^4I_J transitions, the time constant is dramatically decreasing with the concentration. Concerning these transitions, it can be noted that for GaGeSbS-S70 matrix, lifetimes are lower than for 2S2G matrix. Moreover, the measured fluorescence lifetimes do not match the Judd-Ofelt predictions, as it shows millisecond ranged radiative lifetimes. This behavior suggests the presence of hopping migration assisted energy transfer between Nd^{3+} ions, increasing the cross relaxation rate [69,70], which leads to more radiation trapping by the glass impurities.

3.5 Fluorescence of Nd^{3+} ions doped $Ga_5Ge_{20}Sb_{10}S_{65}$ and $Ga_5Ge_{20}Sb_5S_{70}$ fibers

Attenuation has been recorded for an Nd^{3+}-doped 1000 ppmw. $Ga_5Ge_{20}Sb_{10}S_{65}$ fiber. In the Fig. 11, absorption bands corresponding to energy levels $^4I_{15/2}$, $^4I_{13/2}$ and $^4I_{11/2}$ can be observed. The vibration of S-H bonds ([S-H] = 25 ppm, content determined from the bulk preform) gives absorption bands at 3.1 and 4.0 µm. Band at 4.2 µm is attributed to CO_2 vibrations [71]. It can be noted that C-S vibrations band appears generally at 4.95 µm. This band is probably covered by the large band corresponding to the $^4I_{11/2}$ level.

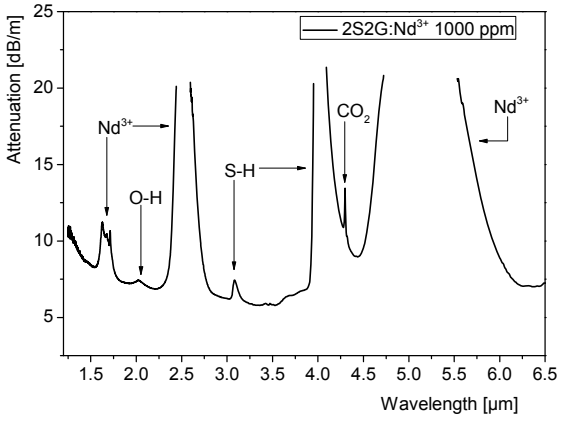

Fig. 11. Attenuation of Nd^{3+}-doped 2S2G fiber ($Ø_{fiber}$ = 350 µm).

Fluorescence emissions were recorded on 4 cm length fibers for several transitions (Fig. 12). We observed six main emission bands corresponding to $^4F_{3/2} \rightarrow {}^4I_{9/2}$, $^4F_{3/2} \rightarrow {}^4I_{11/2}$,

Optical Materials EXPRESS

$^4F_{3/2} \rightarrow {}^4I_{13/2}$, $^4F_{3/2} \rightarrow {}^4I_{15/2}$, $^4I_{13/2} \rightarrow {}^4I_{9/2}$ and $^4I_{15/2} \rightarrow {}^4I_{13/2}$, $^4I_{13/2} \rightarrow {}^4I_{11/2}$, $^4I_{11/2} \rightarrow {}^4I_{9/2}$ transitions at 916, 1095, 1387, 1982, 2560 and 5149 nm respectively. The band at 5 µm was not observed for the $Ga_5Ge_{20}Sb_5S_{70}$ glass matrix for experimental reasons. We can also observe a weak emission corresponding to $^4F_{5/2} + {}^2H_{9/2} \rightarrow {}^4I_{11/2}$ and $^4F_{5/2} + {}^2H_{9/2} \rightarrow {}^4I_{13/2}$ transitions at 1000 and 1225 nm, respectively. The intensities are lower for the $Ga_5Ge_{20}Sb_5S_{70}$ fiber compare to the $Ga_5Ge_{20}Sb_{10}S_{65}$ fiber. This could be explained by the quality of the $Ga_5Ge_{20}Sb_5S_{70}$ fiber whose manufacturing needs to be improved, especially low crystallization appearing during fiber drawing.

Considering the $^4F_{3/2} \rightarrow {}^4I_{15/2}$ transition, the width and the structure of this emission band are due to Stark splitting of manifolds of the two concerned levels. Considering the maximum energy gap between these two levels calculated from the absorption spectra, it is possible to determine a 300 nm width of the emission band. It corresponds to the observed width of the emission band for the $^4F_{3/2} \rightarrow {}^4I_{15/2}$ transition. This observation confirms that the emission band observed can be attributed to the $^4F_{3/2} \rightarrow {}^4I_{15/2}$ transition despite a low branching ratio.

The emission band observed between 2.4 and 2.8 µm corresponds to $^4I_{15/2} \rightarrow {}^4I_{11/2}$ and $^4I_{13/2} \rightarrow {}^4I_{9/2}$ emissions. If we consider the two emitting levels, the $^4I_{13/2}$ level is much more populated by upper levels ($^4F_{5/2}$, $^2H_{9/2}$ and $^4F_{3/2}$) than the $^4I_{15/2}$ level, due to favorable branching ratio (Table 5 and 6). Moreover, the branching ratio of the $^4I_{13/2} \rightarrow {}^4I_{9/2}$ transition is higher than that of the $^4I_{15/2} \rightarrow {}^4I_{11/2}$ transition. These observations are in agreement with a major contribution of the $^4I_{13/2} \rightarrow {}^4I_{9/2}$ transition. A cross-relaxation phenomenon between the involved levels can occur: increasing the population in the $^4I_{13/2}$ and decreasing the population in the $^4I_{15/2}$. This energy transfer is responsible for a dominant transition at 2.5 µm for the $^4I_{13/2} \rightarrow {}^4I_{9/2}$ transition.

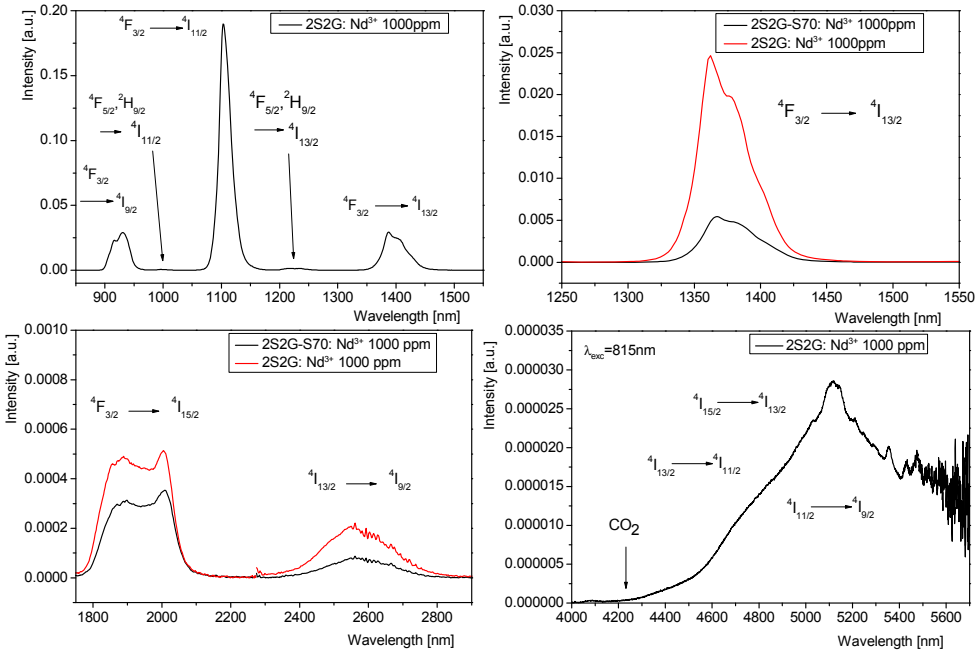

Fig. 12. Emission spectra of $Ga_5Ge_{20}Sb_{10}S_{65}$ and $Ga_5Ge_{20}Sb_5S_{70}$ fiber doped with 1000 ppmw of Nd^{3+}ions.

The neodymium possesses a broad emission band from 4.2 to more than 5.6 µm. This emission band is potentially composed of three contributions corresponding to $^4I_{15/2} \rightarrow {}^4I_{13/2}$, $^4I_{13/2} \rightarrow {}^4I_{11/2}$ and $^4I_{11/2} \rightarrow {}^4I_{9/2}$ transitions. As the $^4I_{15/2}$ level has a low population and the $^4I_{15/2}$

Optical Materials EXPRESS

$\rightarrow {}^4I_{13/2}$ transition has a low branching ratio (18%), this transition is expected in low proportion. The branching ratio for the ${}^4I_{13/2} \rightarrow {}^4I_{11/2}$ transition is about 33% with an emitting level mainly populated compare to the ${}^4I_{15/2}$ level. Finally, due to the strong population of the ${}^4I_{11/2}$ level from upper levels (${}^4F_{3/2}$ and ${}^4I_{15/2}$), the ${}^4I_{11/2} \rightarrow {}^4I_{9/2}$ transition corresponds to the dominant transition of this broad emission band observed.

4. Conclusion

This paper reports some properties of glasses from Ga-Ge-Sb-S system with neodymium ion as rare earth dopant. No significant difference concerning optical band-gap, refractive index, density and T_g have been observed with increase of Nd^{3+} dopant from 500 to 7500 ppmw. The absorption coefficient increases obviously with the amount of Nd_2S_3 inside the glass. The absorption cross-section is still the same, whatever the concentration of rare earth. Characterizations were performed, especially on band-gap, refractive index, chromatic dispersion and T_g, following the composition variation of the matrix in order to improve efficiency of Nd^{3+} fluorescence emission in sulfide glasses. Several compositions of the Ga-Ge-Sb-S system were investigated to shift the band-gap to shorter wavelengths to facilitate the laser pumping. By increasing amount of gallium and antimony, optical band-gap has been shifted from 542 to 601 nm. The T_g increases with raising the ratio Ge/S. The structural analysis using several characterization techniques like Raman scattering spectrometry, NMR of ^{71}Ga and Extended X-Ray Absorption Fine Structure (EXAFS, K-edge of Ga, Ge, Sb and Nd) allows to better understand the structure of the Ga-Ge-Sb-S glasses and the environment of Nd^{3+} ions. Glasses of Ga-Ge-Sb-S system are mainly composed of $[GaS_{4/2}]$ and $[GeS_{4/2}]$ tetrahedra and $[SbS_{3/2}]$ pyramidal units. Depending on their composition, these glasses can present a low proportion of homopolar bonds (mainly S-S, Ge-Ge, Ge-Sb). Two glasses among the investigated compositions, $Ga_5Ge_{20}Sb_{10}S_{65}$ and $Ga_5Ge_{20}Sb_5S_{70}$ presenting interesting properties allowing fiber drawing and the blue-shift of the band-gap, were used for the doping with Nd^{3+} ions. Consequently, absorption cross-sections were analyzed to study the spectroscopy of Nd^{3+} doped $Ga_5Ge_{20}Sb_{10}S_{65}$ and $Ga_5Ge_{20}Sb_5S_{70}$, by means of JO theory. The optical fibers were drawn from the two compositions enabling Nd^{3+} emissions from these fibers. The intensity of emission, with same concentration of rare earth, is lower for $Ga_5Ge_{20}Sb_5S_{70}$ matrix than for $Ga_5Ge_{20}Sb_{10}S_{65}$ glass. The synthesis and fiber drawing of $Ga_5Ge_{20}Sb_5S_{70}$ can be optimized to avoid crystallization and improve the emission efficiency of Nd^{3+} ions. Nevertheless, it must be highlighted that mid-IR emission from $Ga_5Ge_{20}Sb_{10}S_{65}$ fiber was observed presenting broad 4.7-5.7 µm band.

Funding

ADEME, the French Environment & Energy management agency (COPTIK) and Optigas ANR project (ANR-15-CE39-0007)

Acknowledgments

Virginie Nazabal is thankful to Alain Garcia from ICMCB at Bordeaux University for $BaGa_2S_4$ and $CaGa_2S_4$ synthesis for 71-Ga NMR study.